Few of the trends are significant, large surface warming trends are not observed, and like the Western Arctic Ocean analysis in Table 1, significant surface cooling trends are found during winter and autumn. Significant warming trends are observed at the 850 hPa level and the 850–700 hPa layer during winter, in agreement with GCM simulations, but the surface trend is negative. The trends presented in Table 2 are more representative temporally, as they use 36–38 years out of a possible 41, as compared with 20–30 years in the regional analysis (Table 1). On the basis of these tests, we feel that any possible bias introduced by the non-uniform database is small.

The lack of widespread significant warming trends leads us to conclude that there is no strong evidence to support model simulations of greenhouse warming over the Arctic Ocean for the period 1950–1990. Our results, combined with the inconsistent performance of model simulations of Arctic climate[6], indicate a need to understand better the physical processes that affect the polar regions, especially atmosphere–ice–ocean interactions, ocean heat transfer and cloud radiative effects, and to incorporate thermodynamic sea-ice components into future models. We consider the retrieval of temperature profiles from satellite sounding instruments to be an important means of further resolving the spatial and temporal gradients in Arctic air temperatures. □

Received 23 July; accepted 21 December 1992.

1. Houghton, J. T. (ed.) *Climate Change: The IPCC Scientific Assessment* (Cambridge Univ. Press, Cambridge, 1990).
2. Budyko, M. I. *Tellus* **21,** 611–619 (1969).
3. Sellers, W. D. *J. appl. Meteorol.* **8,** 392–400 (1969).
4. Ingram, W. J., Wilson, C. A. & Mitchell, F. J. B. *J. geophys. Res.* **94,** 8609–8622 (1989).
5. Kelly, P. M., Jones, P. D., Sear, C. B., Cherry, B. S. G. & Tavakol, R. K. *Mon. Weath. Rev.* **110,** 71–83 (1982).
6. Hansen, J. & Lebedeff, S. *J. geophys. Res.* **92,** 13345–13372 (1987).
7. Hansen, J. *et al. J. geophys. Res.* **93,** 9341–9364 (1988).
8. Walsh, J. E. & Crane, R. G. *Geophys. Res. Lett.* **19,** 29–32 (1992).
9. Walsh, J. E. & Chapman, W. L. *J. Climate* **3,** 237–250 (1990).
10. Angell, J. K. *Mon. Weath. Rev.* **114,** 1922–1930 (1986).
11. Angell, J. K. & Korshover, J. *Mon. Weath. Rev.* **111,** 901–921 (1983).
12. Karoly, D. J. *Geophys. Res. Lett.* **16,** 465–468 (1989).
13. Kahl, J. D. *et al. J. geophys. Res.* (submitted).
14. Timerev, A. A. & Egorov S. A. *Meterorol. Gidrol.* No. 7, 50–56 (1991).
15. Nagurnyi, A. P., Timerev, A. A. & Egorov, S. A. *Akad. Nauk SSSR, Dokl.* **319,** 1110–1113 (1991).
16. Serreze, M. C., Kahl, J. D. & Schnell, R. C. *J. Climate,* **5,** 615–629 (1992).
17. Serreze, M. C. *et al. J. geophys. Res.* **97,** 9411–9422 (1992).
18. Walsh, J. E. *Mon. Weath. Rev.* **105,** 1527–1535 (1977).
19. Kahl, J. D., Serreze, M. C., Shiotani, S., Skony, S. M. & Schnell, R. C. *Bull. Am. met. Soc.* **73,** 1824–1830 (1992).
20. Serreze, M. C., Kahl, J. D. & Shiotani, S. *National Snow and Ice Data Center spec. Rep. No. 2* (CIRES, University of Colorado, 1992).
21. Skony, S. M. thesis, Univ. of Wisconsin-Milwaukee (1992).
22. Diaconis, P. & Efron, B. *Scient. Am.* **248,** 116–130 (1983).

ACKNOWLEDGEMENTS. Portions of this work were sponsored by the NOAA's Climate and Global Change Program, the Electric Power Research Institute, and the NSF Division of Polar Programs. The project was conducted as part of the US-Russia Joint Committee on Cooperation in Environmental Protection, the Influence of Environmental Change on Climate (Working Group VIII). Helpful comments were provided by A. A. Tsonis.

Detection of crustal deformation from the Landers earthquake sequence using continuous geodetic measurements

Yehuda Bock, Duncan C. Agnew, Peng Fang, Joachim F. Genrich, Bradford H. Hager*, Thomas A. Herring*, Kenneth W. Hudnut†, Robert W. King*, Shawn Larsen‡, J.-Bernard Minster, Keith Stark, Shimon Wdowinski & Frank K. Wyatt

Institute of Geophysics and Planetary Physics, Scripps Institution of Oceanography, La Jolla, California 92093, USA
* Department of Earth, Atmospheric, and Planetary Sciences, Massachusetts Institute of Technology, Cambridge, Massachusetts 02139, USA
† US Geological Survey, Pasadena, California 91106, USA
‡ Scientific Software Division, Lawrence Livermore National Laboratory, Livermore, California 94550, USA

THE measurement of crustal motions in tectonically active regions is being performed increasingly by the satellite-based Global Positioning System (GPS)[1,2], which offers considerable advantages over conventional geodetic techniques[3,4]. Continuously operating GPS arrays with ground-based receivers spaced tens of kilometres apart have been established in central Japan[5,6] and southern California to monitor the spatial and temporal details of crustal deformation. Here we report the first measurements for a major earthquake by a continuously operating GPS network, the Permanent GPS Geodetic Array (PGGA)[7–9] in southern California. The Landers (magnitude M_w of 7.3) and Big Bear (M_w 6.2) earthquakes of 28 June 1992 were monitored by daily observations. Ten weeks of measurements, centred on the earthquake events, indicate significant coseismic motion at all PGGA sites, significant post-seismic motion at one site for two weeks after the earthquakes, and no significant preseismic motion. These measurements demonstrate the potential of GPS monitoring for precise detection of precursory and aftershock seismic deformation in the near and far field.

The PGGA, established in southern California (Fig. 1) in the spring of 1990, is a network of five continuously operating GPS receivers providing an uninterrupted record of crustal motion in near real-time. At each site there is a precise P-code GPS receiver with its antenna mounted on a geodetic monument. Twenty-four hours of data are automatically collected from each site once a day; the operational analysis provides the site position averaged over the day (0–24 h Universal Time Coordinated, UTC), although finer resolution is possible. The precision of the daily relative position between any two sites in the network, based on long-term scatter of nearly 2 years of measurements, is ~5 mm in the horizontal and 10–20 mm in the vertical. To obtain this precision, and to achieve near-real-time solutions, we compute orbits for all GPS satellites, using data collected by a globally distributed network of about 25 permanent tracking stations[10] (Fig. 1), and corrections to tabulated predictions[11] of the orientation of the Earth's rotation axis (polar motion). The worldwide tracking network defines a global reference frame in which coordinates for the PGGA stations, in unstable southern California, can be computed with respect to rigid plate interiors (for example, the North American plate).

Here we report measurements of seismically induced displacements of the PGGA stations due to the Landers (M_w 7.3, 11:58 UTC, 34.22° N, 116.43° W) and Big Bear (M_w 6.2, 15:07 UTC, 34.21° N, 116.83° W) earthquakes of 28 June 1992. We examined the series of PGGA station positions in the 10-week period centred on the day of the earthquakes using a Kalman-filter formulation[12] to analyse the daily 24-hour PGGA solutions. For the day of the earthquakes, we computed the station positions separately from the 12 hours of data before the Landers earthquake and the 9 hours of data after the Big Bear event. The global tracking network was fairly extensive as the 3-month International GPS Service campaign[13] began on 21 June (Fig. 1). Displacements of the PGGA sites, listed in Table 1, were determined by examining the variation in the positions before and after the earthquakes with respect to a global reference frame defined by the coordinates of the tracking network stations. The horizontal displacements of the PGGA sites are

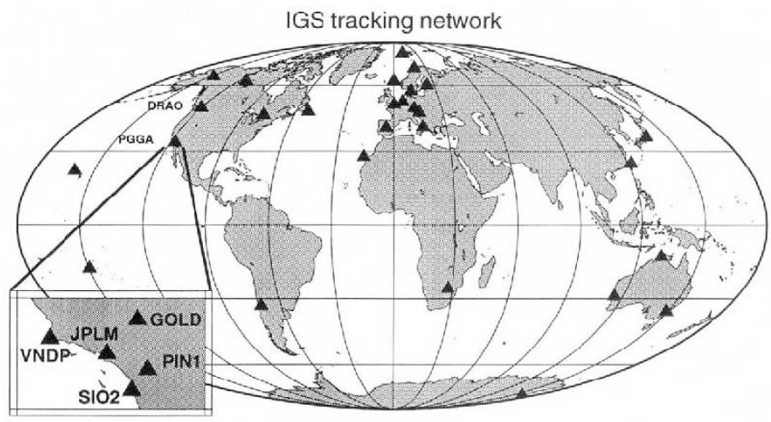

FIG. 1 The distribution of global GPS permanent tracking stations and PGGA sites used for our analysis of observations for the period May–August 1992. The closest tracking site outside California is DRAO in Penticton, British Columbia. All stations use Rogue SNR-8 GPS receivers except for two PGGA sites, SIO2 in La Jolla and VNDP at Vandenberg Air Force Base, which use Ashtech LX-II3 GPS receivers. The global tracking network is usually described by the acronyms CIGNET and FLINN, standing for Cooperative International GPS Network and Fiducial Laboratories for an International Natural science Network[10], and more recently by the International GPS Service (IGS)[13].

plotted in Fig. 2. The maximum horizontal displacement of 48 mm was detected at PIN1, located at the Piñon Flat Observatory (PFO) ~80 km from the seismic rupture zone. In Fig. 3 we take differences for the positions obtained with respect to the global reference frame and plot the daily record of relative horizontal positions between PIN1 and three other stations (Fig. 1). These were a global tracking site (DRAO) near Penticton, British Columbia, Canada, more than 1,700 km to the north and the global tracking station closest to the PGGA; the PGGA site (JPLM) in Pasadena; and the PGGA site (GOLD) at the NASA Deep Space Network Goldstone Complex.

An examination of the station displacements indicates that most of the deformation is due to the coseismic phase of the crustal deformation cycle[14]. The coseismic displacements appear clearly as step functions in the time series of daily station positions (Fig. 3). No significant pre-seismic signature is discernible from the five weeks of daily data taken before the earthquakes. There appears, however, to be a significant post-seismic signature of 0.9 ± 0.3 mm day^{-1} in our estimates of the relative positions of GOLD and PIN1 for 16 days after the earthquakes (Fig. 3). An examination of the displacements at the individual stations indicates that most of the post-seismic motion occurs at GOLD at a rate of 0.7 ± 0.3 mm day^{-1}. (We were concerned that displacements observed at GOLD might stem from the construction of its antenna support, a 12-m-high microwave tower. This station, unlike the other PGGA stations which have very stable geodetic monuments, was neither installed nor operated primarily for monitoring tectonic motions, and might easily be recovering from the mainshock accelerations. Comparing the changing position of this monument with respect to another continuously operating GPS receiver 10 km away indicates, however, that the displacements were tectonic in origin.) The remainder of the motion, ~3 mm in total, occurs at PIN1, but the rate of displacement is not well determined from the data. Greater temporal detail and higher short-term resolution is provided by laser strainmeters at PFO; these show no pre-seismic signal, although post-seismic strains in the first 1–2 weeks following the earthquakes are consistent with our observations at PIN1. Further discrimination of the post-seismic signal will require the implementation of more refined analysis techniques. We intend to study the much longer time series of data before and after the earthquakes to look for possible pre-seismic signals and changes in the interseismic rate of deformation, and to understand better the error spectrum of continuous GPS data. We are currently investigating an increase in

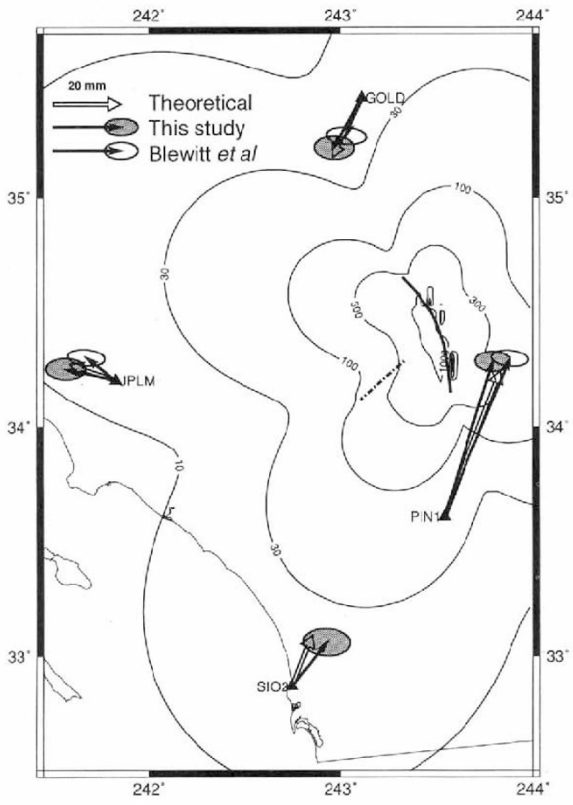

FIG. 2 Observed (solid arrows) and modelled (blank arrows) displacements at the PGGA stations, including 95% confidence ellipses. The observed displacements are calculated with respect to the reference frame defined by the positions and velocities of the global tracking stations, and include the total displacement estimated over the 5-week period after the earthquakes. Except for GOLD and a very small effect at PIN1, the displacements seem to be due entirely to coseismic motion. The total displacement observed at GOLD is 17 mm which includes ~6 mm of coseismic motion and 11 mm of apparent post-seismic motion over the 16 days following the earthquakes. For comparison, we show the displacements and 95% confidence ellipses (unshaded) computed by Blewitt *et al.*[15]. The contours of displacement magnitude, and the calculated displacements are for an elastic halfspace (all units are millimetres). The surface trace of the Landers rupture (heavy line) is composed of six segments with end points at latitude and longitude (degrees) (34.1500, 243.5708), (34.2250, 243.5625), (34.3625, 243.5375), (34.4500, 243.5000), (34.4958, 243.4750), (34.5917, 243.3917) and (34.6542, 243.3208). The magnitudes of slip are 1.5, 3.5, 1.0, 4.8, 5.2 and 0.8 m right-lateral respectively, with all segments from 0 to 15 km depth. The dashed line shows the surface trace assumed for the fault segment of the Big Bear earthquake, with 0.4 m of left-lateral slip on a segment from 3 to 15 km depth, and end points (34.1200, 243.1037) and (34.2884, 243.3297).

TABLE 1 Theoretical and observed displacements

Site	Distance (km)	North (mm) M	North (mm) O	East (mm) M	East (mm) O	Amplitude (mm) M	Amplitude (mm) O	Amplitude (mm) M/O	Azimuth (deg) M	Azimuth (deg) O	Azimuth (deg) M−O	Vertical (mm) M	Vertical (mm) O
PIN1	89	42.8	45.6±1.2	16.2	14.0±2.1	45.8	47.7±2.4	0.96	20.7	17.1	3.6	13.8	9.6±6.4
GOLD	117	−17.5	−14.6±1.4	−8.5	−8.0±2.4	19.5	16.6±2.8	1.17	205.9	208.7	−2.8	7.3	6.0±5.6
JPLM	155	4.7	3.4±1.3	−13.4	−14.7±2.4	14.2	15.1±2.7	0.94	289.3	283.0	6.3	0	0
SIO2	185	15.1	13.0±1.7	6.0	10.1±2.8	16.2	16.5±3.3	0.98	21.7	37.8	−16.1	8.9	10.3±8.2
VNDP	380	0.9	4.5±1.6	−3.0	−4.1±2.5	3.1	6.1±3.0	0.51	286.7	317.7	−31.0	2.6	3.9±5.4

Total displacements in the horizontal components of the PGGA stations computed by a variable slip dislocation model (M) and estimated from 10 weeks of GPS observations (O) centred on the day of the earthquakes, and a comparison of the modelled and observed amplitudes and azimuths of the displacements. The displacements are computed with respect to the global reference frame defined by the global tracking stations (Fig. 1). The errors listed for the observed displacements are 1σ values. The distance from the PGGA sites to the centroid of the model is given. For completeness we include the vertical displacements computed from the dislocation model and estimated from the GPS observations. In this case, the table gives the values for the motion of the PGGA sites relative to JPLM which has been shifted to 0 for both observation and model values. This requires adding 3.7 mm to the model value and 25.9 mm to the observed value. The vertical component errors are not well understood, however, so the agreement with the dislocation model may be fortuitous.

the data noise after the earthquakes (Fig. 3); this may partly be a meteorological effect related to the transition into summer, a phenomenon that has been observed in many years of positions determined by very-long-baseline interferometry in California.

An independent analysis of the PGGA and global tracking data by a group at the Jet Propulsion Laboratory (JPL) yielded

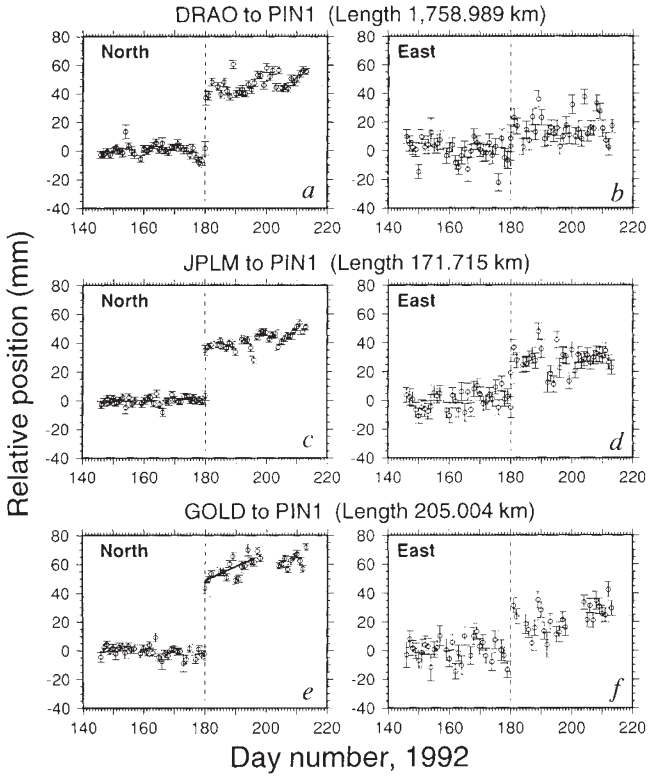

FIG. 3 Time series of daily horizontal relative positions (north and east components) over a 10-week period centred on the day of the earthquakes (day 180, 28 June 1992) for PIN1 relative to DRAO (*a*, *b*), JPLM (*c*, *d*) and GOLD (*e*, *f*). The dotted horizontal lines are determined from the weighted means of the data for the 5-week period before and after the earthquakes, and indicate the coseismic signature (these differ from the Kalman-filter estimates given in Table 1 by not more than 2.5 mm). The error bars have been scaled by a factor of two to account for the effects of correlated noise sources. These are not included in our statistical estimates of the uncertainties, which assume white-noise error sources. In *e*, we fit by least squares a straight line, with a slope of 0.9 ± 0.3 mm day^{-1}, to the apparent post-seismic signature for the 16 days following the earthquakes. The east component has a larger scatter than the north component because the integer-cycle phase ambiguities were not resolved to integer values[16,18] in the daily PGGA solutions.

similar total displacements, as reported by Blewitt *et al.*[15]. The JPL group used the GIPSY GPS software[16,17] to process the data whereas we used the GAMIT/GLOBK GPS software[12,18]. The algorithms used in these two programs were independently developed and use different approaches. Furthermore, the two groups used different global reference frames and different subsets of the global tracking and PGGA data. We analysed ten weeks of data from all five PGGA sites, which included three Rogue SNR-8 GPS receivers and two Ashtech LX-II3 GPS receivers (at VNDP and SIO2), whereas Blewitt *et al.* analysed 8 weeks of Rogue receiver data only. A comparison of the results is shown in Fig. 2. The overlaps of our respective 95% confidence ellipses indicate good agreement at the three common sites.

In Fig. 2 we show the coseismic displacements computed from a variable slip dislocation model in an elastic halfspace[19,20]. The model for the Landers earthquake separates the 65-km rupture into six vertical planar segments (Fig. 2), oriented to coincide with the epicentre and the curvilinear pattern observed in the surface break and aftershock distribution[21]. The right-lateral slip on the southernmost three segments was calculated by averaging over each segment the observed surface offset and the slip distribution obtained by inverting strong-motion seismic data[22]. Slip on the northern three segments was obtained by fitting the displacement vector at GOLD. This required significantly less slip than observed along the surface break. The surface faulting observed geologically continued 10 km to the northwest of the main aftershock zone, suggesting that rupture along this segment of the fault is confined to shallow depths[15,21]. The Big Bear event was modelled as left-lateral rupture along a vertically dipping fault, oriented to coincide with the focal mechanism and aftershock distribution; the slip was chosen to agree with the seismic moment (H. Kanamori, personal communication).

There is good agreement between the theoretical and observed displacements at the PGGA sites (Table 1, Fig. 2). Our fit to the displacement vectors, although nonunique, suggests less slip in the northern half of the Landers rupture. In fact, the geodetic moment calculated using these far-field PGGA data is 0.8×10^{20} N m, which is generally less than moments obtained by independent means: near-field seismic (0.8–0.9×10^{20} N m), geological (0.9×10^{20} N m), near-field geodetic (1.0×10^{20} N m) and teleseismic (1.1×10^{20} N m)[21,23]. The comparatively low PGGA moment may be a manifestation of the influence of the mantle, which has higher values of elastic moduli than the crust[24], so that far-field amplitudes of theoretically computed displacements are reduced relative to homogeneous halfspace models. In this case, the far-field is distances greater than the 30 km thickness of the crust.

These data show that continuous GPS arrays can provide reliable, precise and rapid determination of crustal motion, in particular seismically induced deformation. Although dense spatial coverage with such stations is not economically feasible

at present, advances in GPS receiver technology will allow denser and more continuous measurements. □

Received 17 August; accepted 11 December 1992.

1. Dixon, T. H. *A. Rev. Geophys.* **29,** 249–276 (1991).
2. Hager, B. H., King, R. W. & Murray, M. H. *Rev. Earth planet. Sci.* **19,** 351–382 (1991).
3. Sauber, J., Thatcher, W. & Solomon, S. C. *J. geophys. Res.* **91,** 12683–12693 (1986).
4. Savage, J. *Geophys. Res. Lett.* **17,** 2113–2116 (1990).
5. Shimada, S. *et al. Nature* **343,** 631–633 (1990).
6. Shimada, S. & Bock, Y. *J. geophys. Res.* **97,** 12437–12455 (1992).
7. Bock, Y. & Leppard, N. (eds) *Global Positioning System: An Overview* 40–56 (Springer, New York, 1990).
8. Lindqwister, U., Blewitt, G., Zumberge, J. & Webb, F. *Geophys. Res. Lett.* **18,** 1135–1138 (1991).
9. Bock, Y. *GPS World* (Aster, Eugene, Oregon, 1991).
10. Minster, J.-B., Hager, B. H., Prescott, W. H. & Schutz, R. E. *International Global Network of Fiducial Stations* (National Res. Council, National Academy Press, Washington DC, 1991).
11. International Earth Rotation Service *Bulletins B 51-54* (Observatoire de Paris, 1992); *Bulletins A Vol. V* (U.S. Naval Observatory, 1992).
12. Herring, T. H., Davis, J. L. & Shapiro, I. I. *J. geophys. Res.* **95,** 12561–12583 (1990).
13. Beutler, G. *Eos* **73,** 134 (1992).
14. Scholz, C. H. *The Mechanics of Earthquakes and Faulting* (Cambridge Univ. Press, 1990).
15. Blewitt, G. *et al. Nature* **361,** 340–342 (1993).
16. Blewitt, G. *J. geophys. Res.* **94,** 10187–10203 (1989).
17. Blewitt, G. *Geophys. Res. Lett.* **17,** 199–202 (1990).
18. Dong, D. & Bock, Y. *J. geophys. Res.* **94,** 3949–3966 (1989).
19. Mansinha, L. & Smylie, D. E. *Bull. seism. Soc. Am.* **61,** 1433–1440 (1971).
20. Okada, Y. *Bull. seism. Soc. Am.* **75,** 1135–1154 (1985).
21. Landers Earthquake Response Team *Science* (submitted).
22. Kanamori, H., Thio, H.-K., Dreger, D., Hauksson, E. & Heaton, T. *Geophys. Res. Lett.* **19,** 2267–2270 (1992).
23. Hudnut, K. W. *et al. Eos* **73,** 365 (1992).
24. Rybicki, K. *Bull. Seism. Soc. Am.* **61,** 79 (1971).

ACKNOWLEDGEMENTS. We thank K. Feigl and J. Savage for reviews, H. Kanamori for assistance, our colleagues at JPL, especially S. Dinardo, for maintaining the quality of the PGGA and much of the global tracking network, and G. Blewitt for assistance in comparing results. We thank the US National Geodetic Survey and Energy, Mines and Resources Canada, and the participants in the international GPS campaign (IGS) for data and resources. Supported by NASA, NSF, the Southern California Earthquake Center, the US Geological Survey and the US Air Force Office of Scientific Research. S.L.'s work was done under the auspices of the US Dept. of Energy by the Lawrence Livermore National Laboratory. Y.B.'s work was done in part through a Scripps/JPL joint appointment.

Absolute far-field displacements from the 28 June 1992 Landers earthquake sequence

Geoffrey Blewitt, Michael B. Heflin, Kenneth J. Hurst, David C. Jefferson, Frank H. Webb & James F. Zumberge

Jet Propulsion Laboratory, California Institute of Technology, Pasadena, California 91109, USA

ON 28 June 1992, the largest earthquake in California in 40 years (surface-wave magnitude $M_s = 7.5$) occurred near the small town of Landers, in southeastern California, and was followed three hours later by the nearby M_s 6.5 Big Bear earthquake[1]. Fortuitously, the Landers earthquake sequence coincided with the first week of the official three-month test period of the International Global Positioning System and Geodynamics Service[2] (IGS), giving us an unprecendented opportunity to detect absolute pre-, co- and post-seismic displacements at a distance of 50–200 km from the main rupture with millimetre-level precision. Mutual and independent confirmation of some of our geodetic results are demonstrated by Bock *et al.* in this issue[3]. For the Landers earthquake, the observed displacements indicate that the depth of the bottom of the rupture is shallower towards the northern end, displacements were dominantly symmetric, and the rupture extended further south on the Johnson Valley fault than has been mapped on the basis of surface ground offsets. The combined geodetic moment for the Landers and Big Bear earthquakes (1.1×10^{20} N m^{-1}) agrees well with teleseismic estimates.

The Landers and Big Bear earthquakes and their aftershocks occurred along faults that form a triangle bounded to the southwest by the San Andreas fault (Fig. 1). Extensive surface rupture resulting from these events has been reported along the Johnson Valley and Camp Rock/Emerson faults. Ground breakage occurs along a 70-km stretch of these faults, reaching a maximum surface offset of 6.7 m (ref. 1). The Landers earthquake occurred toward the southern end of the hypothesized 'Mojave shear zone', which trends N 35° W across the Mojave Desert, into Owens Valley and the northern Basin and Range province[4,5]. This zone reportedly carries 7–8 mm yr^{-1} of the relative motion between the Pacific and North American plates, and may be a manifestation of a subcrustal fault[4,5]. Aftershocks following the Landers earthquake line up along this apparent shear zone from as far south as the San Andreas fault, to further north than our station GOLD shown in Fig. 1. The pattern of aftershocks is sparse on the Camp Rock fault segment which underlies the northernmost 13 km of the visible surface rupture[6]. Using a new geodetic tool for earthquake studies, we have estimated permanent surface displacements in southern California due to the cumulative effect of events on 28 June, and show that geodetic methods provide valuable information on aspects of the rupture mechanism not available with other techniques. We also offer an explanation for the unexpected lack of aftershocks on the Camp Rock fault.

Since 21 June 1992, a worldwide network of stations has been routinely receiving precise microwave ranging data from the United States Department of Defence's 18-satellite Global Positioning System (GPS)[7], and transmitting the data to IGS data centres to be made available to analysis centres and geodynamics researchers. Regional GPS networks benefit from the precise orbit determination and reference frame stability supplied by an extensive tracking network[8–10]. A regional array of receivers operated jointly by the Jet Propulsion Laboratory (JPL) and Scripps Institution of Oceanography has been operational in southern California since 1990 (ref. 11). A simultaneous analysis of GPS data from the California array combined with the global network data has allowed us to estimate the absolute displacements, in the international terrestrial reference frame[12] (ITRF), of three stations located within 50–200 km from the Landers earthquake rupture, with 2-mm precision in the horizontal plane.

To reduce systematic errors that can be introduced by mixing different types of GPS receivers and antennas, we have analysed

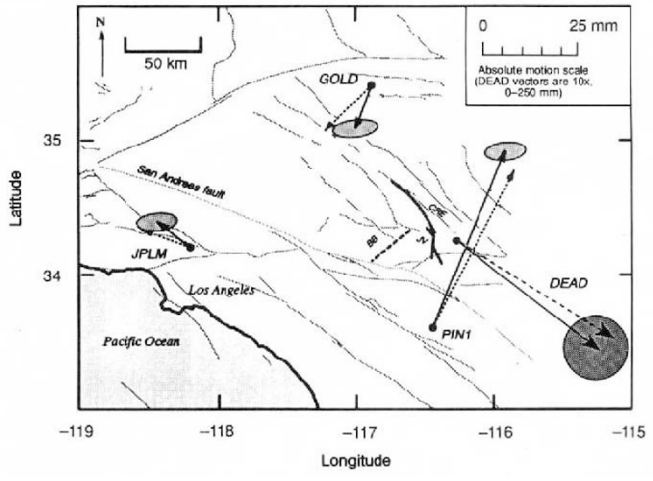

FIG. 1 Map showing absolute motions of Goldstone (GOLD), Pasadena (JPLM), Pinyon Flat (PIN1) and Deadman (DEAD). Solid arrows are the observed displacements with 95% confidence regions. The vectors and confidence region for DEAD is shown at 0.1 times the scale of the other stations. The model displacements, assuming an elastic half-space, are shown as dashed arrows. The surface trace of the model of the Landers earthquake is shown by the solid heavy line. Dashed heavy line (BB) is the trace of the fault used to model the Big Bear earthquake. Shaded solid and dashed lines are active faults in the region: JV is the Johnson Valley fault; CRE is the Camp Rock/Emerson fault.